This article has been accepted for publication in a future issue of this journal, but has not been fully edited. Content may change prior to final publication. Citation information: DOI 10.1109/TTE.2021.3109093, IEEE Transactions on Transportation Electrification

Open-Switch and Current Sensor Fault Diagnosis Strategy for Matrix Converter Based PMSM Drive System

Hanbing Dan, Wei Yue, Wenjing Xiong, Yonglu Liu, Mei Su, *Member, IEEE*, Yao Sun, *Member, IEEE*

***Abstract*—Reliable fault diagnosis and identification are essential for permanent magnet synchronous motor (PMSM) drive system with high reliability requirements. Since open-switch fault and output current sensor fault both affect the residual of output phase current, it is difficult to identify them apart from each other. Thus, this paper proposes an open-switch fault and output current sensor fault diagnosis and identification method for matrix converter (MC) based PMSM drive system. The finite control set model predictive control (FCS-MPC) method is applied in MC based PMSM drive system. The fault identification method is proposed based on the extracted different faulty features of open-switch fault and output current sensor fault. After the open-switch fault is separated from the current sensor fault, an error-voltage based open-switch fault diagnosis strategy is applied to locate the faulty switch. Hardware-in-the-loop tests are carried out to verify the effectiveness of the proposed method.**

***Index Terms*—Current sensor faults, finite control set-model predictive control, fault diagnosis, fault identification, matrix converter, open-switch faults, permanent magnet synchronous motor.**

I. Introduction

THE matrix converter (MC) [1], [2] has a spacious application prospect in the field of motor drive systems due to its excellent electrical properties, such as no huge dc-link capacitor and low harmonic pollution to power gird. Permanent magnet synchronous motor (PMSM) is widely applied in manufacturing industries due to its small size, high efficiency, and high-power density. The MC based PMSM drive system is widely used in airplanes, electric ships, and military vehicles[3] due to these advantages. However, electrical faults that happened in MC will cause cascading accidents, which results in enormous losses to industrial production. There are many kinds of faults in motor drive system. Among which, 38% of faults are power circuit faults [4], and most power circuit faults are power switch faults and sensor faults. Power switch faults can be divided into open-circuit or short-circuit faults [5]. Generally, a short-circuit fault can be transformed into an open-circuit fault by a series fuse to avoid catastrophic consequences. Apart from power switch in motor drive system, sensors are essential to provide critical feedback information for the control of the system. However, the sensor fault may lead to the deviation of the system feedback, which deteriorates the performance of motor drive system and causes secondary faults of the system. Therefore, the fast and reliable diagnosis method is extremely important to ensure the safe operation of the system.

Until now, numerous fault detection and isolation (FDI) methods have been proposed [6]. Most open-switch fault diagnosis methods are analyzed for voltage source inverter (VSI) drive system. Wavelet analysis is widely used as a typical method in signal processing-based fault diagnosis strategies [7]-[9]. Other signal processing methods for detecting open-switch faults include Fast Fourier Transform (FFT) [10] and fuzzy technique [11]. The hardware cost is low as no extra sensor is added. However, it is relatively complex and time-consuming. Some open-switch fault diagnosis methods based on average normalized currents have been proposed for VSI in [12]-[16]. This kind of approach [12] requires only the measured currents of load side, and the open-switch faults can be detected with a relatively small amount of calculation. In [13] and [14], the characteristic of stator average normalized currents is utilized. All sorts of open-switch faults can be diagnosed, which is independent of the system control scheme. In [15], by innovatively combining the fuzzy-based fault diagnosis method with the phase current information, the intermittent faults can be also detected. M. Trabelsi et al. proposed an open-switch fault diagnosis strategy combining the information of line currents shapes in αβ frame and their normalized mean values [16]. However, the identification variable is hard to define. In [17], a robust open-switch fault diagnosis method based on the common mode voltages of the inverter in induction motor drive systems is proposed, and an active common-mode voltage injection method to enhance diagnostic reliability is presented.

There is some research about the open-switch fault diagnosis method for the MC drive system. Faulty features are extracted from the information of measured output current, clamp current and line-to-line voltage. In [18], an open-switch fault diagnosis

Manuscript received January 23, 2021; revised March 15, 2021 and June 27, 2021; accepted August 25, 2021. This work was supported in part by the Hunan Provincial Key Laboratory of Power Electronics Equipment and Grid under Grant 2018TP1001, in part by the National Natural Science Foundation of China under Grant 61903382, 51807206, 61933011, in part by the Major Project of Changzhutan Self-Dependent Innovation Demonstration Area under Grant 2018XK2002, in part by the Project of Innovation-driven Plan in Central South University under Grant 2019CX003, in part by the Fundamental Research Funds for the Central Universities of Central South University under Grant 206021703. (Corresponding author: Wenjing Xiong).

Hanbing Dan, Wei Yue, Wenjing Xiong, Yonglu Liu, Mei Su, and Yao Sun are with the Hunan Provincial Key Laboratory of Power Electronics Equipment and Gird, School of Automation, Central South University, Changsha, 410083 China (email: daniel698@sina.cn, 194612118@csu.edu.cn, csu.xiong@163.com, liuyonglu@csu.edu.cn, sumeicsu@csu.edu.cn, yaosuncsu@gmail.com).

This article has been accepted for publication in a future issue of this journal, but has not been fully edited. Content may change prior to final publication. Citation information: DOI 10.1109/TTE.2021.3109093, IEEE Transactions on Transportation Electrification

approach based on monitoring output phase current and switch state is proposed, it is simple to diagnose the exact location of the open-switch in MC with finite control set-model predictive control (FCS-MPC). However, this method is time-consuming. In [19], the proposed fault diagnosis method can locate the faulty switch by comparing the clamp current with the output phase current. However, its computation burden is largely due to the massive integral operation. In [20], the proposed fault diagnosis method moves the current sensors ahead of the clamp circuit connection. The faulty switch can be diagnosed by sampling the information during the zero vector of each modulation period. In [21], an error-voltage based open-switch fault diagnosis strategy is proposed. This strategy can quickly locate the faulty switch according to the line-to-line voltage residuals. However, only three phase balanced resistance-inductance load is considered. This diagnosis strategy is applied in this manuscript for the open-switch fault diagnosis of MC based PMSM drive system.

Sensor faults can be more catastrophic in motor drive system. Therefore, various fault diagnosis methods for current sensor faults have been proposed. Observer-based methods are extensively used to diagnose the sensor faults in the whole motor drive system. In [22], a sensor fault diagnosis strategy is proposed by subtracting the feedback output phase current value from the reference value, and a single-phase current sensor encoderless control scheme is also introduced based on a sliding-mode observer. A simplified calculation method is proposed by changing the stationary coordinate frame [23]. To diagnose the faults of different position sensors timely, three independent observers are established to observe the values of speed, DC voltage and output current respectively [24]. After a sensor fault is detected, the system operates with the remaining sensors. However, the design of observers is complicated. In [25], a new fault diagnosis and tolerant method based on dual sliding-mode observers is proposed. After the fault diagnosis, those sliding-mode observers are utilized to reconstruct the fault current and estimate the rotor position respectively. In [26], a flux-linkage observer-based current estimation scheme is proposed to detect current sensor faults for direct torque control of induction motor. Yong Yu et al propose a fault detection scheme of current sensor fault by integrating three independent observers [27]. A complete sensor FDI strategy has been proposed based on the Extended Kalman Filter (EKF) for induction motor drive system [28] and interior permanent-magnet synchronous motor (IPMSM) drive system [29]. T. A. Najafabadi et al [30] propose an FDI strategy for induction motor drives based on an adaptive observer, which relies on the accuracy of the estimated rotor-resistance. It increases the robustness of the whole fault diagnosis method. Additionally, a current sensor FDI strategy based on online estimation of rotor and stator resistances is proposed for induction motor [31].

Open-switch faults and current sensor faults have homologous faulty characteristics. These two kinds of faults can cause distortion in the estimated output currents and estimated output voltages. That is why the existing fault diagnosis methods only aim at one kind of fault. To identify the open-switch fault with the current sensor fault, a fault diagnosis and tolerant method for dual three-phase drive PMSM system are proposed in [32]. Based on the characteristics of direct torque control and space vector modulation, multiple observers are constructed, and a full set of FDI strategies are proposed. However, the diagnosis process is complicated. Zhan Li et al. propose a fault diagnosis method for three-phase three-wire inverter [33]. It innovatively combines line-to-line voltage deviations and phase voltage deviations to extract unique faulty characteristics. However, the system cost is increased due to additional voltage sensors.

In conclusion, there is little research on the open-switch and current sensor faults diagnosis method applied to the MC based PMSM drive system. The direct MC has nine groups of switches, and the input voltage of MC is variable. Thus, the open-switch and current sensor faults diagnosis of MC is

difficult. By innovatively combining current residuals and line-to-line voltage residuals, this paper proposes an open-switch and current sensor fault diagnosis method for MC based PMSM drive system with FCS-MPC to locate the faulty switch and the faulty current sensor. The faulty switch and the faulty current sensor are identified without extra sensors. This paper is organized as follows. Section II describes the topology and control strategy of the MC based PMSM drive system. Section III describes the detailed implementation process of the proposed fault diagnosis method. Hardware-in-the-loop (HIL) tests are presented in Section IV. The conclusion is obtained in Section V.

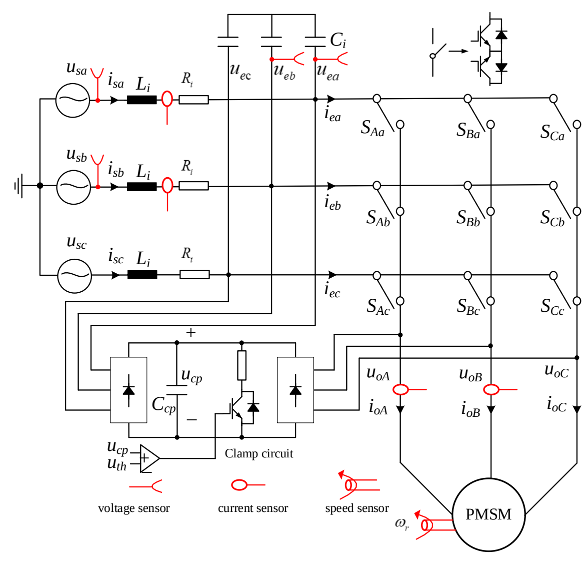

Fig. 1. Diagram of MC based PMSM drive system.

II. Modeling and Control for MC System

A. MC topology

The structure of the whole system is shown in Fig. 1, which is composed of three-phase balanced source supply, MC and PMSM. The MC consists of a three-phase LC filter, nine bidirectional switches and a clamp circuit. The three-phase LC filter is employed to attenuate the switching frequency harmonics. The clamp circuit connects the load side to the three-phase source, which consists of 12 fast-recovery diodes to connect the clamping capacitor between the input and output terminals. It can provide the current path in case of system failure, meanwhile, it prevents the circuit from overvoltage.

This article has been accepted for publication in a future issue of this journal, but has not been fully edited. Content may change prior to final publication. Citation information: DOI 10.1109/TTE.2021.3109093, IEEE Transactions on Transportation Electrification

It is forbidden that the load is connected in an open circuit or the power source is connected in a short circuit. Thus, the switching state of the MC needs to satisfy the following constraints:

$$\begin{cases} S_{Aa}+S_{Ab}+S_{Ac}=1 \\ S_{Ba}+S_{Bb}+S_{Bc}=1 \\ S_{Ca}+S_{Cb}+S_{Cc}=1 \end{cases} \tag{1}$$

while $S_{Xy}(X\in\{A,B,C\}, y\in\{a,b,c\})=1$ represents S_{Xy} is turned ON, $S_{Xy}=0$ represents S_{Xy} is turned OFF. Therefore, the MC possesses 27 valid switching states. Accordingly, the reference output line-to-line voltage can be represented by input voltage and switching state as follows:

$$\begin{bmatrix} u_{oAB}^* \\ u_{oBC}^* \\ u_{oCA}^* \end{bmatrix}=\begin{bmatrix} S_{Aa}-S_{Ba} & S_{Ab}-S_{Bb} & S_{Ac}-S_{Bc} \\ S_{Ba}-S_{Ca} & S_{Bb}-S_{Cb} & S_{Bc}-S_{Cc} \\ S_{Ca}-S_{Aa} & S_{Cb}-S_{Ab} & S_{Cc}-S_{Ac} \end{bmatrix}\begin{bmatrix} u_{ea} \\ u_{eb} \\ u_{ec} \end{bmatrix} \tag{2}$$

The input current can be represented by output current and switching state as follows:

$$\begin{bmatrix} i_{ea} \\ i_{eb} \\ i_{ec} \end{bmatrix}=\begin{bmatrix} S_{Aa} & S_{Ab} & S_{Ac} \\ S_{Ba} & S_{Bb} & S_{Bc} \\ S_{Ca} & S_{Cb} & S_{Cc} \end{bmatrix}^T\begin{bmatrix} i_{oA} \\ i_{oB} \\ i_{oC} \end{bmatrix} \tag{3}$$

B. Model of MC based PMSM drive system

Fig. 2 depicts the control block diagram of the whole MC based PMSM drive system, it mainly includes the FCS-MPC and an outer loop. In this scheme, i_d^* is set to zero, and i_q^* is obtained by speed loop proportional-integral (PI) regulator. The target of MC-based PMSM drive system is to obtain the desired speed and unity power factor. FCS-MPC is applied to track the reference of output current and source current.

The continuous-time model of the input filter can be expressed as:

$$\begin{bmatrix} \dfrac{du_e}{dt} \\ \dfrac{di_s}{dt} \end{bmatrix}=A\begin{bmatrix} u_e \\ i_s \end{bmatrix}+B\begin{bmatrix} u_s \\ i_e \end{bmatrix} \tag{4}$$

$$\begin{bmatrix} u_{oA} \\ u_{oB} \\ u_{oC} \end{bmatrix}=\begin{bmatrix} S_{Aa} & S_{Ab} & S_{Ac} \\ S_{Ba} & S_{Bb} & S_{Bc} \\ S_{Ca} & S_{Cb} & S_{Cc} \end{bmatrix}\begin{bmatrix} u_{ea} \\ u_{eb} \\ u_{ec} \end{bmatrix} \tag{5}$$

where $A=\begin{bmatrix} 0 & \frac{1}{C_i} \\ -\frac{1}{L_i} & -\frac{R_i}{L_i} \end{bmatrix}$, $B=\begin{bmatrix} 0 & \frac{1}{C_i} \\ \frac{1}{L_i} & 0 \end{bmatrix}$, and R_i, L_i, C_i represent the resistor, inductance, and capacitance of the input filter, respectively; u_e and i_e represent the input voltage and input current respectively; u_s and i_s represent the source voltage and source current respectively.

The discrete model is given as:

$$\begin{bmatrix} u_e^{k+1} \\ i_s^{k+1} \end{bmatrix}=G\begin{bmatrix} u_e^{k} \\ i_s^{k} \end{bmatrix}+H\begin{bmatrix} u_s^{k} \\ i_e^{k} \end{bmatrix} \tag{6}$$

where $G=e^{AT_s}$, $H=A^{-1}(G-I)B$, T_s represents the sampling period.

The state-space equation in discrete state of PMSM model is given as:

$$\begin{cases} u_d^k=R_s i_d^{k-1}+L_d\dfrac{i_d^k-i_d^{k-1}}{T_s}-\omega_e^k L_q i_q^{k-1} \\ u_q^k=R_s i_q^{k-1}+L_q\dfrac{i_q^k-i_q^{k-1}}{T_s}+\omega_e^k\left(L_d i_d^{k-1}+\psi_f\right) \end{cases} \tag{7}$$

where the superscript '*k*' and '*k*-1' represent the value at the *k-th* and (*k*-1)-*th* sampling period, respectively; where ψ_f represents the magnet flux linkage; i_d^k and i_q^k represent stator current of *d-q* axis, which is obtained by Park transform with i_{oA}, i_{oB}, i_{oC}; R_s represents the resistance of stator, L_d and L_q represent *d-q* axis inductance respectively; u_d^k and u_q^k represent the stator voltage of *d-q* axis; ω_e^k represents the electric angular velocity.

The *d-q* axis current equation in discrete state can be obtained by (7):

$$\begin{cases} i_d^k=\left(1-\dfrac{R_sT_s}{L_d}\right)i_d^{k-1}+\dfrac{\omega_e^kT_sL_q}{L_d}i_q^{k-1}+\dfrac{T_s}{L_d}u_d^k \\ i_q^k=\left(1-\dfrac{R_sT_s}{L_q}\right)i_q^{k-1}-\dfrac{\omega_e^kT_sL_d}{L_q}i_d^{k-1}+\dfrac{T_s}{L_q}u_q^k-\dfrac{\omega_e^kT_s\psi_f}{L_q} \end{cases} \tag{8}$$

C. Control strategy

The sinusoidal source current and unity power factor are required for MC based PMSM system in most application filed [2]. The following conditions are assumed:

1)The input resistance is small and neglected.

2) The input power factor is unity.

3) The system efficiency is η.

According to the law of power conservation, the root mean square (RMS) value of reference source current can be expressed as follows:

$$I_{rms}^*=\frac{\hat{T}_e\omega_m}{3\eta U_{rms}} \tag{9}$$

where ω_m represents the mechanical angular velocity of the PMSM, and U_{rms} is the RMS value of source voltage.

The estimated electromagnetic torque can be obtained as follows:

$$\hat{T}_e=\frac{3n_p}{2}\left(\psi_f i_q^k+\left(L_d-L_q\right)i_d^k i_q^k\right) \tag{10}$$

where n_p represents the number of pole pairs. The reference value of source current can be given by

$$i_s^*=\left[\sqrt{2}I_{rms}^*\cos\varphi \quad \sqrt{2}I_{rms}^*\cos\left(\varphi-\frac{2\pi}{3}\right) \quad \sqrt{2}I_{rms}^*\cos\left(\varphi+\frac{2\pi}{3}\right)\right]^T \tag{11}$$

The choice of the cost function is a key point in the implementation of FCS-MPC. To control the MC based PMSM drive system, the cost function must take the variables of both sides of the converter into account.

On the input filter side, the cost function can be expressed as follows to ensure a sinusoidal source current and a unity power factor:

$$\Delta i=\left(i_{s\alpha}^{k+1}-i_{s\alpha}^*\right)^2+\left(i_{s\beta}^{k+1}-i_{s\beta}^*\right)^2 \tag{12}$$

where $i_{s\alpha}^{k+1}$ and $i_{s\beta}^{k+1}$ represent the predictive values of the source current in α-β axis, and $i_{s\alpha}^*$,$i_{s\beta}^*$ are the reference values of the source current in α-β axis.

This article has been accepted for publication in a future issue of this journal, but has not been fully edited. Content may change prior to final publication. Citation information: DOI 10.1109/TTE.2021.3109093, IEEE Transactions on Transportation Electrification

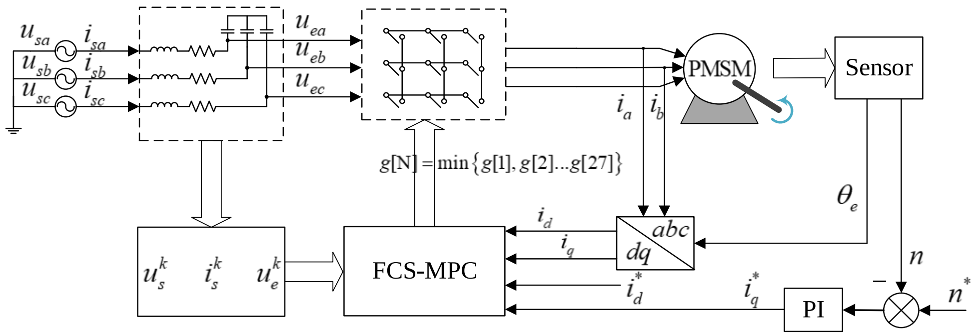

Fig. 2. Control block diagram for MC-based PMSM system.

On the PMSM load side, the main objective is the speed tracking of PMSM. The proportional-integral (PI) speed controller as shown in Fig. 2 is used to track the reference rotor speed. The output current is controlled by FCS-MPC to track the reference value i_d^* and i_q^*. Combined with (12), the cost function is chosen as:

$$g = \lambda_1 \left(i_d^{k+1} - i_d^*\right)^2 + \lambda_2 \left(i_q^{k+1} - i_q^*\right)^2 + \Delta i \tag{13}$$

where λ_1 and λ_2 represent the weighting factors of cost function, and the weighting factor λ is empirically adjusted [34], i_d^{k+1} and i_q^{k+1} represent the predictive values of *d*-*q* axis output current, i_d^* and i_q^* represent the reference values of *d*-*q* axis output current. At each sampling period, 27 effective switching states are evaluated to calculate 27 corresponding cost function values.

The switching state corresponding to the minimum cost function value is applied in the next sampling period.

$$g[N] = \min\{g[1], g[2], ..., g[i], ..., g[27]\} \tag{14}$$

III. Proposed Fault Diagnosis Strategy

A. Fault identification method

The faulty features of the open-switch fault and the current sensor fault are analyzed. A fault identification method is proposed based on the extracted different faulty features. When the fault occurs in the output phase current sensor, the residuals between the current feedback value and the actual value become a large value. According to the discrete mathematical model of the motor, the estimated *d*-*q* axis current value can be obtained by equation (8).

The estimated current of output phase current is transformed as:

$$\begin{bmatrix} \hat{i}_{oA} \\ \hat{i}_{oB} \\ \hat{i}_{oC} \end{bmatrix} = \begin{bmatrix} \cos\theta & -\sin\theta \\ \cos\left(\theta - \frac{2\pi}{3}\right) & -\sin\left(\theta - \frac{2\pi}{3}\right) \\ \cos\left(\theta - \frac{4\pi}{3}\right) & -\sin\left(\theta - \frac{4\pi}{3}\right) \end{bmatrix} \begin{bmatrix} \hat{i}_d \\ \hat{i}_q \end{bmatrix} \tag{15}$$

where $\hat{i}_{oA}$, $\hat{i}_{oB}$ and $\hat{i}_{oC}$ are the estimated output current value, respectively; and θ is the rotor flux orientation angle.

The feedback values of output current i_{oA_fdb} and i_{oB_fdb} are obtained from the output current sensors in phase A and phase B, respectively. The current residuals between the estimated value and feedback value are calculated according to equation (16). The residuals are ideally zero during normal operation. When the current sensor is faulty, the absolute values of current residuals will be larger than a positive value ε_1. The sum of absolute values $|\varepsilon_{sensor\_a}|$ and $|\varepsilon_{sensor\_b}|$ will be larger than a positive value ε_0. ε_0 and ε_1 are selected to minimize the possibility of false alarms caused by the noises.

$$\begin{cases} \varepsilon_{sensor\_a} = \hat{i}_{oA} - i_{oA\_\mathrm{fdb}} \\ \varepsilon_{sensor\_b} = \hat{i}_{oB} - i_{oB\_\mathrm{fdb}} \end{cases} \tag{16}$$

When the MC happens an open-switch fault and the current sensor is normal, the actual output line-to-line voltage will be different from the reference output line-to-line voltage. Then the difference will lead to a large deviation between the estimated and feedback value of output current. Although the current sensor is normal, there is still a large difference between the estimated value and the feedback value of the output current, which results in misdiagnosis. Therefore, this manuscript proposes a diagnostic method to identify the open-switch fault and the current sensor fault from each other according to the deviation between estimated and feedback value of output current.

The PMSM could be simplified as a three-phase symmetrical load with back EMF. The output port of MC is equivalent to a controlled voltage source. Assume that the switch S_{Aa} is suffering an open-switch fault, the actual output voltage u_{oA} is divided into the reference voltage u_{oA}^* and faulty component voltage Δu_{oA}. And the equation $u_{oA} = u_{oA}^* + \Delta u_{oA}$ is satisfied, Δu_{oA} generates the current component Δi_{oA}. The equivalent circuit is shown in Fig. 3(a). According to the superposition theorem, the equivalent circuit in Fig. 3(a) is divided to two equivalent circuits in Fig. 3(b). Since the load is symmetrical, the current produced by faulty component voltage Δu_{oA} will be evenly distributed to phase B and phase C, then, $\Delta i_{oA} = 2\Delta i_{oB} = 2\Delta i_{oC}$. Similarly, it can be derived that $\Delta i_{oB} = 2\Delta i_{oA} = 2\Delta i_{oC}$ when the phase B happens an open-switch fault, and $\Delta i_{oC} = 2\Delta i_{oA} = 2\Delta i_{oB}$ when the open-switch fault happens in phase C. Practically, to avoid the false alarm due to noises and parameter uncertainties, a positive threshold value ε_2 is set.

However, the above special faulty feature is not satisfied when the output current sensor is faulty. Thus, the special faulty feature between current components $\Delta i_{oA}, \Delta i_{oB}, \Delta i_{oC}$ in different phases is used to identify the open-switch fault and the

TABLE I
RESIDUALS UNDER DIFFERENT FAULT CONDITIONS

Residuals	Faulty location
$\lvert\varepsilon_{\text{sensor\_a}}\rvert + \lvert\varepsilon_{\text{sensor\_b}}\rvert < \varepsilon_0$	Normal
$\lvert\varepsilon_{\text{sensor\_a}}\rvert + \lvert\varepsilon_{\text{sensor\_b}}\rvert \geq \varepsilon_0$; $\lvert\varepsilon_{\text{sensor\_a}}\rvert \geq \varepsilon_1$, $\lvert\varepsilon_{\text{sensor\_b}}\rvert < \varepsilon_1$	Faulty current sensor in phase A
$\lvert\varepsilon_{\text{sensor\_a}}\rvert + \lvert\varepsilon_{\text{sensor\_b}}\rvert \geq \varepsilon_0$; $\lvert\varepsilon_{\text{sensor\_a}}\rvert < \varepsilon_1$, $\lvert\varepsilon_{\text{sensor\_b}}\rvert \geq \varepsilon_1$	Faulty current sensor in phase B
$\lvert\varepsilon_{\text{sensor\_a}}\rvert + \lvert\varepsilon_{\text{sensor\_b}}\rvert \geq \varepsilon_0$; $\lvert\varepsilon_{\text{sensor\_a}}\rvert \geq \varepsilon_1$,$\lvert\varepsilon_{\text{sensor\_b}}\rvert \geq \varepsilon_1$; $\big\lvert\lvert\varepsilon_{\text{sensor\_a}}\rvert - 2\lvert\varepsilon_{\text{sensor\_b}}\rvert\big\rvert < \varepsilon_2$	Faulty switch in phase A of MC
$\lvert\varepsilon_{\text{sensor\_a}}\rvert + \lvert\varepsilon_{\text{sensor\_b}}\rvert \geq \varepsilon_0$; $\lvert\varepsilon_{\text{sensor\_a}}\rvert \geq \varepsilon_1$,$\lvert\varepsilon_{\text{sensor\_b}}\rvert \geq \varepsilon_1$; $\big\lvert 2\lvert\varepsilon_{\text{sensor\_a}}\rvert - \lvert\varepsilon_{\text{sensor\_b}}\rvert\big\rvert < \varepsilon_2$	Faulty switch in phase B of MC
$\lvert\varepsilon_{\text{sensor\_a}}\rvert + \lvert\varepsilon_{\text{sensor\_b}}\rvert \geq \varepsilon_0$; $\lvert\varepsilon_{\text{sensor\_a}}\rvert \geq \varepsilon_1$,$\lvert\varepsilon_{\text{sensor\_b}}\rvert \geq \varepsilon_1$; $\big\lvert\lvert\varepsilon_{\text{sensor\_a}}\rvert - \lvert\varepsilon_{\text{sensor\_b}}\rvert\big\rvert < \varepsilon_2$	Faulty switch in phase C of MC
$\lvert\varepsilon_{\text{sensor\_a}}\rvert + \lvert\varepsilon_{\text{sensor\_b}}\rvert \geq \varepsilon_0$; $\lvert\varepsilon_{\text{sensor\_a}}\rvert \geq \varepsilon_1$,$\lvert\varepsilon_{\text{sensor\_b}}\rvert \geq \varepsilon_1$; $\big\lvert\lvert\varepsilon_{\text{sensor\_a}}\rvert - 2\lvert\varepsilon_{\text{sensor\_b}}\rvert\big\rvert \geq \varepsilon_2$; $\big\lvert 2\lvert\varepsilon_{\text{sensor\_a}}\rvert - \lvert\varepsilon_{\text{sensor\_b}}\rvert\big\rvert \geq \varepsilon_2$; $\big\lvert\lvert\varepsilon_{\text{sensor\_a}}\rvert - \lvert\varepsilon_{\text{sensor\_b}}\rvert\big\rvert \geq \varepsilon_2$	Faulty current sensors in phase A and B

current sensor fault. The different faulty features for fault location are summarized in Table I.

B. Output current sensor fault diagnosis method

The ground fault of the current sensor is considered. In this case, the output of the faulty sensor sends a value equal to zero to the PMSM controller. The flow chart of the proposed fault diagnosis method for open-switch fault and current sensor fault is shown in Fig. 4. The residual value of current sensor is generated firstly. The sum of absolute values $\lvert\varepsilon_{sensor\_a}\rvert + \lvert\varepsilon_{sensor\_b}\rvert$ is compared with the threshold value ε_0. If the inequation $\lvert\varepsilon_{sensor\_a}\rvert + \lvert\varepsilon_{sensor\_b}\rvert > \varepsilon_0$ is satisfied for some consecutive sampling periods, the fault status of MC-based PMSM system can be detected.

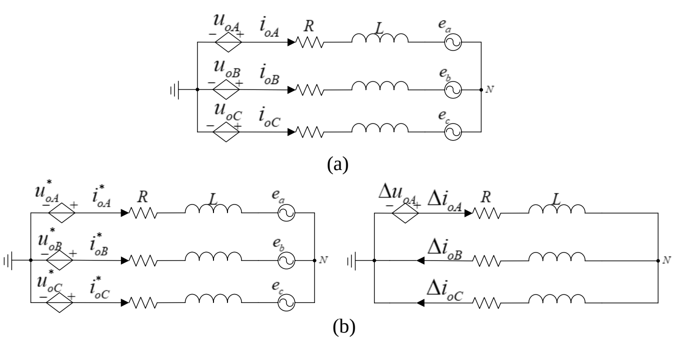

Fig. 3. (a) Equivalent circuit (b) Divided Equivalent circuits.

According to Table I, when the current residual value of one phase exceeds the threshold ε_1 and the other phase does not exceed the threshold ε_1, the phase where the current residual value exceeds the threshold value can be diagnosed as a faulty current sensor. Further judgement is necessary if the two current residuals $\lvert\varepsilon_{sensor\_a}\rvert$ and $\lvert\varepsilon_{sensor\_b}\rvert$ exceed the threshold value, because this situation may be caused by two current sensors failure or switch failure. According to the analysis of Section III-A, the open-switch fault has special properties. $\lvert\varepsilon_{\text{sensor\_a}}\rvert = 2\lvert\varepsilon_{\text{sensor\_b}}\rvert$ when phase A happens an open-switch fault, $2\lvert\varepsilon_{\text{sensor\_a}}\rvert = \lvert\varepsilon_{\text{sensor\_b}}\rvert$ when the phase B happens an open-switch fault, and $\lvert\varepsilon_{\text{sensor\_a}}\rvert = \lvert\varepsilon_{\text{sensor\_b}}\rvert$ when the open-switch fault happens in phase C. If two output current sensors fail, the above relationship will not exist. Accordingly, two current sensor faults can be identified.

If the current sensor is faulty, the fault diagnosis process is finished. If the faulty switch phase leg is detected and separated from the faulty current sensors, the faulty switch detection method is discussed in Section C below.

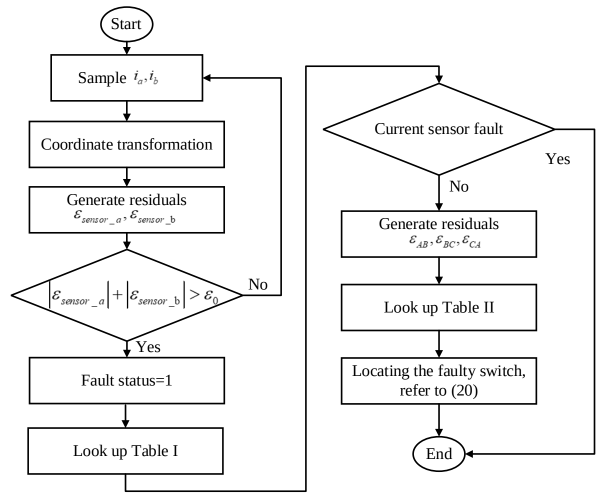

Fig. 4. Flow chart of fault diagnosis method.

C. Open-switch fault diagnosis method

After the open-switch fault is separated from the current sensor fault, a fault diagnosis method [21] based on line-to-line voltage residuals is applied to determine the location of the faulty switch. Utilizing the information of output current, the actual output line-to-line voltages are estimated without additional voltage sensors. Under normal conditions, the residual between the estimated line-to-line voltage and reference line-to-line voltage is close to zero. When an open-switch fault occurs, the estimated line-to-line voltage will be different from the reference line-to-line voltage. This characteristic can be used for open-switch fault diagnosis.

According to (7), the estimated *d-q* axis voltage is obtained as:

$$\begin{cases} \hat{u}_d^k = R_s i_d^{k-1} + L_d \dfrac{i_d^k - i_d^{k-1}}{T_s} - \omega_e^k L_q i_q^{k-1} \\ \hat{u}_q^k = R_s i_q^{k-1} + L_q \dfrac{i_q^k - i_q^{k-1}}{T_s} + \omega_e^k \left(L_d i_d^{k-1} + \psi_f \right) \end{cases} \tag{17}$$

where $\hat{u}_d^k$ and $\hat{u}_q^k$ represent the estimated values of *d-q* axis voltage.

The estimated value and reference value of line-to-line voltage are compared to formulate residual error, and the

TABLE II

RESIDUALS UNDER NORMAL AND FAULTY CONDITIONS

Normal	Faulty switch in phase A $(F_A = 1, F_B = 0, F_C = 0)$	Faulty switch in phase B $(F_A = 0, F_B = 1, F_C = 0)$	Faulty switch in phase C $(F_A = 0, F_B = 0, F_C = 1)$
$\varepsilon_{AB} < \varepsilon_3$	$\varepsilon_{AB} \geq \varepsilon_3$	$\varepsilon_{AB} \geq \varepsilon_3$	$\varepsilon_{AB} < \varepsilon_3$
$\varepsilon_{BC} < \varepsilon_3$	$\varepsilon_{BC} < \varepsilon_3$	$\varepsilon_{BC} \geq \varepsilon_3$	$\varepsilon_{BC} \geq \varepsilon_3$
$\varepsilon_{CA} < \varepsilon_3$	$\varepsilon_{CA} \geq \varepsilon_3$	$\varepsilon_{CA} < \varepsilon_3$	$\varepsilon_{CA} \geq \varepsilon_3$

specific position of the faulty switch phase leg can be detected according to the characteristics of output voltage residuals.

$$\begin{cases} \hat{u}_{oAB} = -\sqrt{3}\hat{u}_d \sin\left(\theta - \frac{\pi}{3}\right) - \sqrt{3}\hat{u}_q \cos\left(\theta - \frac{\pi}{3}\right) \\ \hat{u}_{oBC} = \sqrt{3}\hat{u}_d \sin\theta + \sqrt{3}\hat{u}_q \cos\theta \\ \hat{u}_{oCA} = -\sqrt{3}\hat{u}_d \sin\left(\theta + \frac{\pi}{3}\right) - \sqrt{3}\hat{u}_q \cos\left(\theta + \frac{\pi}{3}\right) \end{cases} \tag{18}$$

The reference values of the output line-to-line voltage can be calculated from equation (2), and the residuals can be defined as:

$$\begin{cases} \varepsilon_{AB} = \left| u_{oAB}^* - \hat{u}_{oAB} \right| \\ \varepsilon_{BC} = \left| u_{oBC}^* - \hat{u}_{oBC} \right| \\ \varepsilon_{CA} = \left| u_{oCA}^* - \hat{u}_{oCA} \right| \end{cases} \tag{19}$$

The machine nonlinearities mainly refer to the parameter variations of resistance, inductance and magnet flux linkage, which can affect the threshold value selection. The threshold value ε_3 is defined considering the variations of inductance and resistance, and the magnet flux linkage is assumed to be a constant. The estimated voltage of *d-q* axis considering parameter variations is represented as $\hat{u}_d'^k$ and $\hat{u}_q'^k$, which can be calculated as:

$$\begin{cases} \hat{u}_d'^k = \hat{R}_s i_d^{k-1} + \hat{L}_d \frac{i_d^k - i_d^{k-1}}{T_s} - \omega_e^k \hat{L}_q i_q^{k-1} \\ \hat{u}_q'^k = \hat{R}_s i_q^{k-1} + \hat{L}_q \frac{i_q^k - i_q^{k-1}}{T_s} + \omega_e^k \left(\hat{L}_d i_d^{k-1} + \psi_f \right) \end{cases} \tag{20}$$

The errors Δu_d^k and Δu_q^k can be obtained by subtracting (17) from (20) as follows:

$$\begin{cases} \Delta u_d^k = \Delta R_s i_d^{k-1} + \Delta L_d \frac{i_d^k - i_d^{k-1}}{T_s} - \Delta L_q \omega_e^k i_q^{k-1} \\ \Delta u_q^k = \Delta R_s i_q^{k-1} + \Delta L_q \frac{i_q^k - i_q^{k-1}}{T_s} + \Delta L_d \omega_e^k i_d^{k-1} \end{cases} \tag{21}$$

where $\Delta R_s, \Delta L_d, \Delta L_q$ represent the errors between the actual value and the estimated value. According to (21), the error value $\Delta\hat{u}_{AB}$ of estimated line-to-line voltage can be calculated as follow:

$$\begin{aligned} \Delta\hat{u}_{AB} &= \sqrt{3}\sqrt{\left(\Delta u_d^k\right)^2 + \left(\Delta u_q^k\right)^2} \sin\left(\theta - \frac{\pi}{3} - \varphi\right) \\ &\leq \sqrt{3}\sqrt{\left(\Delta u_d^k\right)^2 + \left(\Delta u_q^k\right)^2} \end{aligned} \tag{22}$$

where θ is the rotor flux orientation angle, $\varphi = arctan\frac{\Delta u_q^k}{\Delta u_d^k}$.

Assume the variation of machine parameters is in a certain range, the maximum error value of estimated line-to-line voltage considering the parameter variation can be calculated according to equations (21) and (22). Thus, the threshold value ε_3 should be bigger than the maximum estimated line-to-line voltage error value.

The key to locating the open-switch faulty phase leg is summarized in Table II. The residuals (ε_{AB}, ε_{BC} and ε_{CA}) under normal and faulty situations are illustrated. $F_X (X \in A, B, C)$ equals to "1" represents that the open-switch fault happens in phase X, and $F_X (X \in A, B, C)$ equals to "0" represents phase X is normal. Thus, the faulty switch phase leg is located.

Since the FCS-MPC has the known and unchanged switching state, the faulty switch is located with the information of the switching state. The applied switch of the faulty switch phase in the corresponding sampling period can be regarded as the faulty switch. The specific fault location algorithm is as follows:

$$\begin{bmatrix} F_{Aa} & F_{Ab} & F_{Ac} \\ F_{Ba} & F_{Bb} & F_{Bc} \\ F_{Ca} & F_{Cb} & F_{Cc} \end{bmatrix} = \begin{bmatrix} F_A & 0 & 0 \\ 0 & F_B & 0 \\ 0 & 0 & F_C \end{bmatrix} \begin{bmatrix} S_{Aa} & S_{Ab} & S_{Ac} \\ S_{Ba} & S_{Bb} & S_{Bc} \\ S_{Ca} & S_{Cb} & S_{Cc} \end{bmatrix} \tag{23}$$

where $F_{Xy} (X \in \{A, B, C\}, y \in \{a, b, c\})$ equals to "1" when S_{Xy} is open-switch and equals to "0" when S_{Xy} is normal.

IV. HIL RESULTS

Due to the danger that might be caused by the faulty converter, the HIL tests based on OPAL-RT(OP4510) are carried out to verify the effectiveness of the proposed method. The setup of the HIL test system is shown in Fig. 5. The hardware configuration is imported to the host PC through RT-LAB software. The motor model is emulated by MATLAB/SIMULINK, and the non-linearities are ignored. The oscilloscope records the fault diagnosis results. The parameters of each component are shown in Table III. To attenuate harmonics from the power source, a small passive damping resistor R_p is paralleled with L_i. The ideal switching elements are used to replace the bidirectional switches in the MC, and the dead time effect in the switching process is neglected.

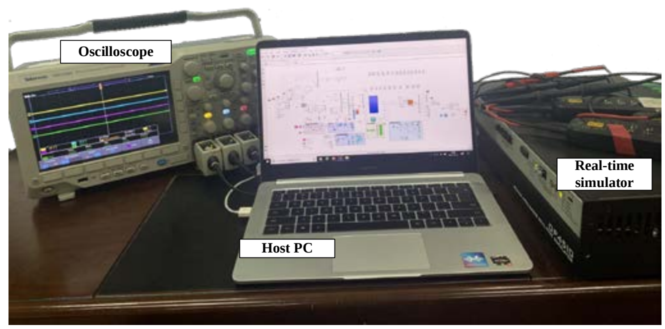

Fig. 5. Setup of HIL test system

This article has been accepted for publication in a future issue of this journal, but has not been fully edited. Content may change prior to final publication. Citation information: DOI 10.1109/TTE.2021.3109093, IEEE Transactions on Transportation Electrification

TABLE III
PARAMETER OF THE HIL TEST

Parameter	Symbol	Value
Source phase voltage	u_s	220 V
frequency	f_{in}	50 Hz
Sampling period	T_s	20 μs
Number of poles	P	2
Filter inductor	L_i	0.5 mH
Filter capacitor	C_i	22 μH
Filter resistor	R_i	0.1 Ω
Passive damping resistor	R_p	9 Ω
Stator resistance	R_s	2.4 Ω
Viscous damping	F	0.05 N·m·s/rad
Inertia	J	0.1 Kg·m^2
Magnet flux linkage	λ_f	0.99 Wb
d-axis inductance	L_d	8.6822 mH
q-axis inductance	L_q	10.4686 mH
Reference speed	$n*$	1000 rpm
Load torque	T_L	10 N·m

A. Effect of parameter variations

To minimize the possibility of false alarms caused by the parameter variations, the threshold values of ε_0, ε_1, ε_2, ε_3 are selected as positive values. Mathematically, the lower bound of the threshold must be greater than the largest absolute value of the three residuals in all possible normal operating conditions. And its upper bound must be less than the minimum absolute value of the three residuals in all possible abnormal operating conditions.

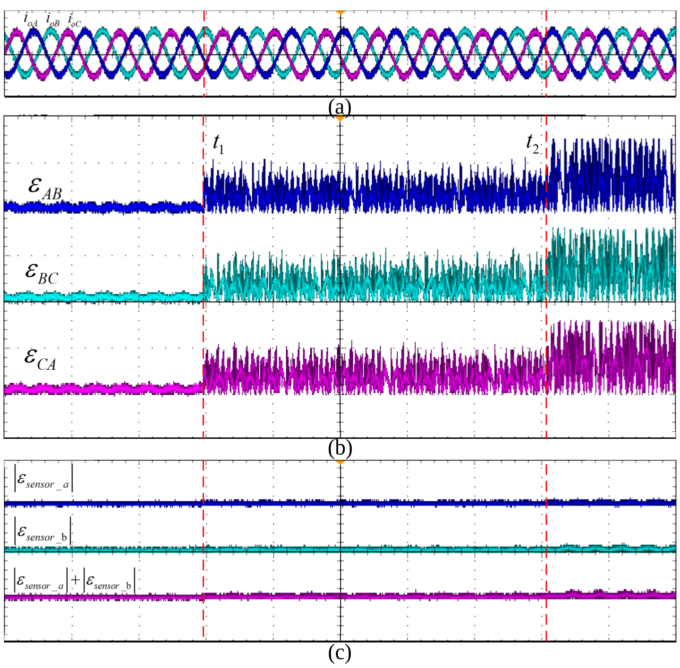

Fig. 6. HIL results of the effect of parameter variations. (a)Three-phase load currents (Ch1: [10A/div], Ch2: [10A/div], Ch3: [10A/div]) (b)Voltage residuals (Ch1: [50V/div], Ch2: [50V/div]), Ch3: [50V/div] (c) Current residuals (Ch1: [10A/div], Ch2: [10A/div], Ch3: [10A/div]), Time: [40ms/div].

The effect of parameter variations on the residuals is shown in Fig. 6. the system model has 10% parameters deviation relative to nominal parameters (stator resistance R_s, d-axis inductance L_d, q-axis inductance L_q) of the real plant between the time t_1 and t_2, and the residuals of line-to-line voltage increase to about 50V. After time t_2, 20% parameter deviation is applied to the motor model, the residuals of line-to-line voltage increase to nearly 80V. The results show that the larger parameter deviation will lead to the increase of residuals inevitably. The threshold ε_3 is set to 100, which can meet the validity of proposed method under the condition of 20% parameter deviation. The current residual is less sensitive to the parameters, so the appropriate threshold ε_0, ε_1 and ε_2 are selected as 15, 10 and 10 to make them greater than their values in most normal operating conditions respectively. However, larger parameter deviation will still lead to false diagnosis of the method, which can be suppressed by further increasing the threshold.

B. Normal operation

The reference speed of PMSM is set to 1000rpm, the load torque is 10N.m. When the MC-based PMSM drive system operates with FCS-MPC method under the normal condition, the HIL results are shown in Fig. 7 and Fig. 8. As seen, the output current is sinusoidal and the unity input power factor is obtained. In addition, the reference output line-to-line voltage almost coincides with the estimated output line-to-line voltage.

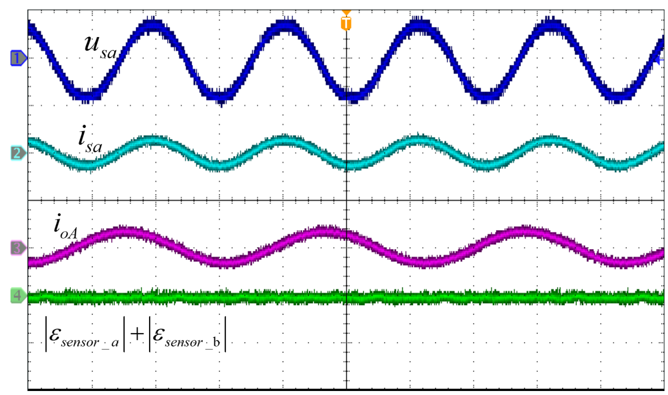

Fig. 7. HIL results during normal condition under 1000r/min,10N.m. (Ch1: [400V/div], Ch2: [10/div], Ch3: [10/div], Ch4: [10A/div]), Time: [10ms/div].

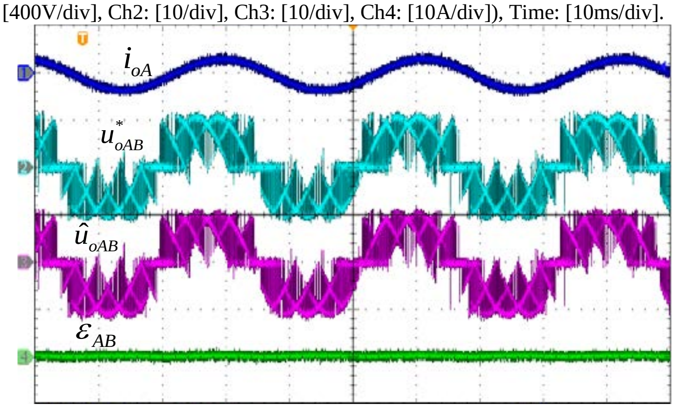

Fig. 8. HIL results during normal condition under 1000r/min,10N.m. (Ch1: [10A/div], Ch2: [500V/div], Ch3: [500V/div], Ch4: [500V/div]), Time: [10ms/div].

Fig. 9 shows the experimental results under the transient and load variations. In Fig.9(e), the PMSM starts from 0r/min and accelerates to 1000r/min, the PMSM load is suddenly changed from 0N.m to 5N.m during acceleration. It can be seen that the current residuals and line-to-line voltage residuals are nearly equal to 0. To ensure the robustness of fault diagnosis method, four positive constant thresholds are selected, $\varepsilon_0 = 15, \varepsilon_1 = 10, \varepsilon_2 = 10, \varepsilon_3 = 100$. As shown in Fig. 9, the sum of

This article has been accepted for publication in a future issue of this journal, but has not been fully edited. Content may change prior to final publication. Citation information: DOI 10.1109/TTE.2021.3109093, IEEE Transactions on Transportation Electrification

$|\varepsilon_{sensor\_a}|$ and $|\varepsilon_{sensor\_b}|$ is less than ε_0, and ε_{AB}, ε_{BC}, ε_{CA} are less than ε_3. Thus, there is no occurrence of misdiagnosis.

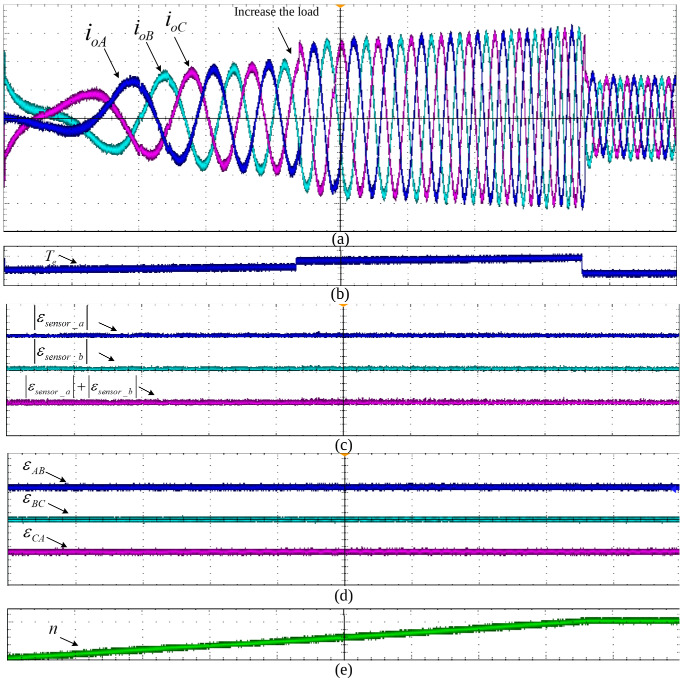

Fig. 9. HIL results of PMSM system from 0 to 1000r/min, 5N.m. (a)Three-phase load currents [2.5A/div] (b)Electromagnetic torque [30N.m/div] (c)Current residuals [5A/div] (d)Three line-to-line voltage residuals [300V/div] (e)Speed of PMSM [1000rpm/div], Time: [100ms/div].

C. Faulty current sensor in phase A

Fig. 10 shows the HIL results of MC based PMSM drive system during normal and phase-A current sensor faulty operation. When the phase-A current sensor is healthy, the speed of PMSM maintains stable and the stator current is sinusoidal with low distortion. The estimated current and feedback current of phases A and B are almost the same, and the residuals are below ε_1. When the phase-A current sensor is faulty, the feedback value of phase-A current is set to zero to simulate the sensor faulty. As a result, the electromagnetic torque contains massive high frequency components, and the integral calculation will have a certain filtering effect on the ripple of electromagnetic torque. Therefore, it has little effect on motor speed. The three-phase stator current is distorted, and the difference between the estimated current value of phase A and the feedback value becomes larger. The sum of the two residuals is greater than the threshold, $|\varepsilon_{sensor\_a}| + |\varepsilon_{sensor\_b}| \geq \varepsilon_0$, which represents that the fault exists. Meanwhile, the inequation $|\varepsilon_{sensor\_a}| \geq \varepsilon_1$ and $|\varepsilon_{sensor_b}| < \varepsilon_1$are satisfied. According to Table I, the fault of the phase A current sensor can be detected.

D. Faulty current sensors in phase A and B

Fig. 11 shows the HIL results of MC based PMSM drive system during normal and both current sensors faulty operation. When phase-A current sensor and phase-B current sensor are faulty, the feedback values of phase-A current and phase-B current are set to zero to simulate the sensor faulty. The residuals of phase-A current sensor and phase-B current sensor

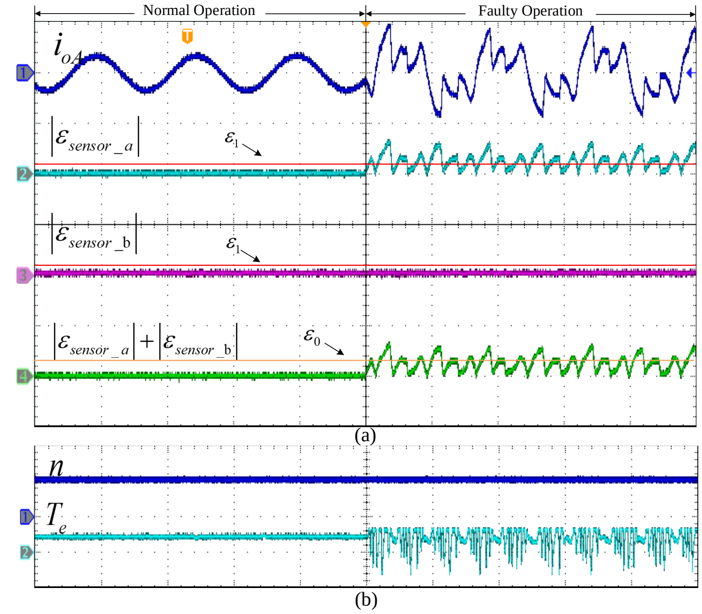

Fig. 10. HIL results during normal and phase-A current sensor faulty operation under 1000r/min,10N.m. (a)Current residuals (Ch1: [25A/div], Ch2: [50A/div], Ch3: [50A/div], Ch4: [50A/div]) (b)Speed and electromagnetic torque (Ch1: [1000rpm/div], Ch2: [25N.m/div]), Time: [40ms/div].

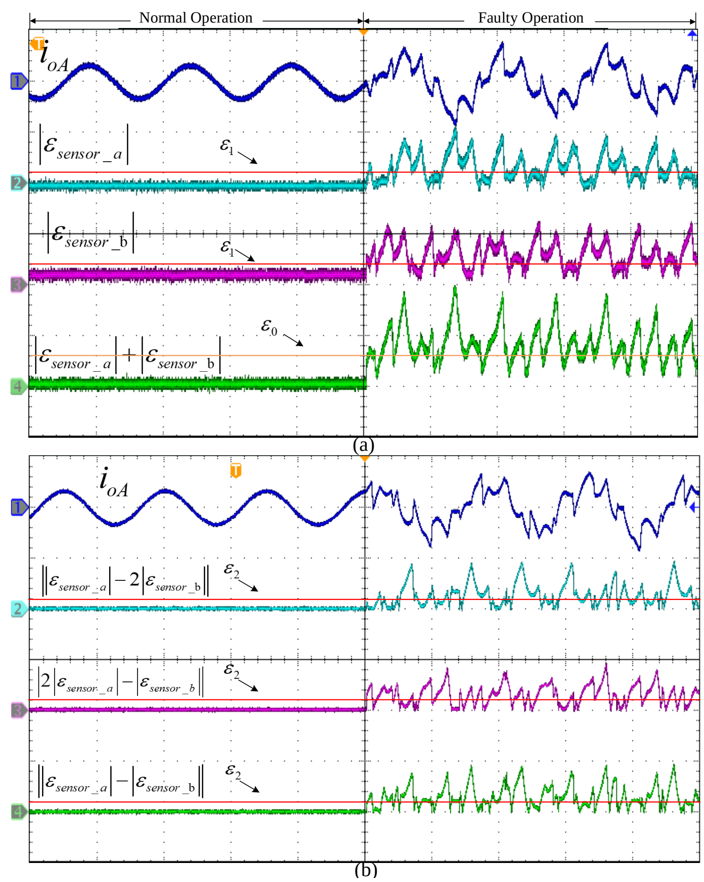

Fig. 11. HIL results during normal and both current sensors faulty operation under 1000r/min,10N.m. (a)Current residuals (Ch1: [25A/div], Ch2: [25A/div], Ch3: [25A/div], Ch4: [25A/div]) (b)The relation of different current residual (Ch1: [25A/div], Ch2: [50A/div], Ch3: [50A/div], Ch4: [50A/div]), Time: [20ms/div].

will increase respectively. The sum of the two residuals is greater than the threshold. Meanwhile, the inequation $\big||\varepsilon_{sensor\_a}| - 2|\varepsilon_{sensor\_b}|\big| \geq \varepsilon_2$, $\big|2|\varepsilon_{sensor\_a}| - |\varepsilon_{sensor\_b}|\big| \geq$

This article has been accepted for publication in a future issue of this journal, but has not been fully edited. Content may change prior to final publication. Citation information: DOI 10.1109/TTE.2021.3109093, IEEE Transactions on Transportation Electrification

ε_2 and $\left||\varepsilon_{\mathrm{sensor\_a}}| - |\varepsilon_{\mathrm{sensor\_b}}|\right| \geq \varepsilon_2$ are satisfied as show in Fig 11(b). According to Table I, phase-A current sensor and phase-B current sensor are faulty.

E. Open-switch Fault in switch S_{Aa}

Fig. 12(a) and Fig. 12(b) depict the performance of the fault diagnosis algorithm. Fig. 12(c) shows the speed and electromagnetic torque of MC based PMSM drive system during normal and switch S_{Aa} faulty operation. When the open-switch fault occurs at the switch S_{Aa}, the values of $|\varepsilon_{\mathrm{sensor\_a}}|$ and $|\varepsilon_{\mathrm{sensor\_b}}|$ increase. Meanwhile, the inequation $|\varepsilon_{\mathrm{sensor\_a}}| + |\varepsilon_{\mathrm{sensor\_b}}| \geq \varepsilon_0$ and $\left||\varepsilon_{\mathrm{sensor\_a}}| - 2|\varepsilon_{\mathrm{sensor\_b}}|\right| < \varepsilon_2$ are satisfied. It is concluded that the open-switch fault is separated and happened in phase A according to Table I.

Fig. 13 shows the HIL results of the MC based PMSM drive system during normal and switch S_{Aa} faulty operation. During normal operation, the estimated line-to-line voltage is coincided with the reference line-to-line voltage, three residuals ε_{AB},ε_{BC} and ε_{CA} are all below the threshold value. During faulty operation, S_{Aa} remains "OFF" although the controller intends to give an "ON" signal to it. The actual output line-to-line voltage is different from the reference output line-to-line voltage. Consequently, the residual errors ε_{AB} and ε_{CA} exceed the threshold, and $(S_{Aa} = 1)$ && $(\varepsilon_{AB} > \varepsilon_3)$ && $(\varepsilon_{BC} \leq \varepsilon_3)$&& $(\varepsilon_{CA} > \varepsilon_3)$, F_{Aa} equal to "1" which reveals that there is an open-switch fault happened in S_{Aa}.

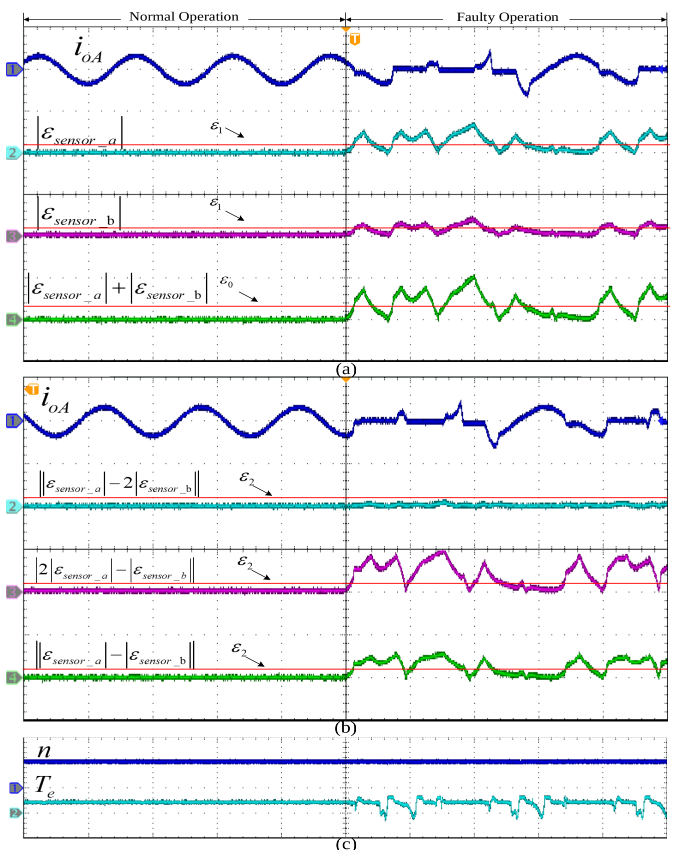

Fig. 12. HIL results during normal and S_{Aa} faulty operation under 1000r/min,10N.m. (a) Current residuals (Ch1: [25A/div], Ch2: [50A/div], Ch3: [50A/div], Ch4: [50A/div]) (b) The relation of different current residual (Ch1: [25A/div], Ch2: [50A/div], Ch3: [50A/div], Ch4: [50A/div]). (c) Speed and electromagnetic torque (Ch1: [1000rpm/div], Ch2: [25N.m/div]), Time: [20ms/div].

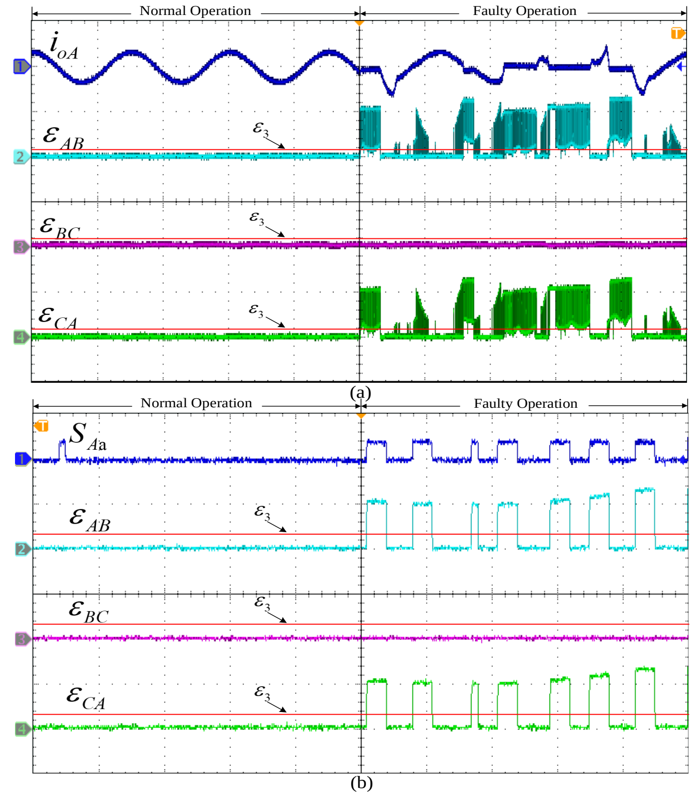

Fig. 13. HIL results during normal and S_{Aa} faulty operation under 1000r/min,10N.m. (a)Voltage residuals (Ch1: [25V/div], Ch2: [600V/div], Ch3: [600V/div], Ch4: [600V/div]), Time: [20ms/div]] (b) The Enlarged drawing of S_{Aa} drive signal and Voltage residuals (Ch1: [2.5V/div], Ch2: [300V/div], Ch3: [300V/div], Ch4: [300V/div]), Time: [200us/div].

V. Conclusion

The open-switch fault and output current sensor fault of MC based PMSM drive system is difficult to be identified due to similar faulty characteristics. To address this issue, a fault identification method of the faulty switch phase leg and the faulty current sensor is proposed by extracting different faulty features from output current residuals. According to the established residual characteristic in Table I and Table II, the specific faulty device can be located. The proposed fault diagnosis and the fault identification strategies are simple and cost-saving without any redundant hardware. Finally, HIL tests demonstrate the feasibility and effectiveness of the proposed fault diagnosis strategy. Besides, the threshold is selected considering the inaccuracy of motor parameters in the HIL test system. However, the machine nonlinearity in real experimental condition is the limitation of the proposed fault diagnosis. It will be meaningful work to apply the proposed fault diagnosis method in real experiment in the future.

REFERENCES

[1] E. Yamamoto, H Hara and T Uchino, "Development of MCs and its Applications in Industry," in *IEEE Industrial Electronics Magazine*, vol. 5, no. 1, pp. 4-12, March 2011.

[2] P. W. Wheeler, J. Rodriguez, J. C. Clare, L. Empringham and A. Weinstein, "Matrix converters: a technology review," in *IEEE Transactions on Industrial Electronics*, vol. 49, no. 2, pp. 276-288, April 2002.

[3] C. Klumpner, P. Nielsen, I. Boldea and F. Blaabjerg, "A new matrix converter motor (MCM) for industry applications," in *IEEE Transactions on Industrial Electronics*, vol. 49, no. 2, pp. 325-335, April 2002.

[4] L. Empringham, J. W. Kolar, J. Rodriguez, P. W. Wheeler and J. C. Clare, "Technological Issues and Industrial Application of Matrix Converters: A Review," in *IEEE Transactions on Industrial Electronics*, vol. 60, no. 10, pp. 4260-4271, Oct. 2013.

[5] R. Wu, F. Blaabjerg, H. Wang, M. Liserre and F. Iannuzzo, "Catastrophic failure and fault-tolerant design of IGBT power electronic converters - an overview," IECON 2013 - 39th *Annual Conference of the IEEE Industrial Electronics Society*, Vienna, 2013, pp. 507-513.

[6] I. Jlassi and A. J. M. Cardoso, "A Single Method for Multiple IGBT, Current, and Speed Sensor Faults Diagnosis in Regenerative PMSM Drives," in *IEEE Journal of Emerging and Selected Topics in Power Electronics*, vol. 8, no. 3, pp. 2583-2599, Sept. 2020.

[7] C. Gan, J. Wu, S. Yang, Y. Hu and W. Cao, "Wavelet Packet Decomposition-Based Fault Diagnosis Scheme for SRM Drives With a Single Current Sensor," in *IEEE Transactions on Energy Conversion*, vol. 31, no. 1, pp. 303-313, March 2016.

[8] Z. Huang, Z. Wang and H. Zhang, "A Diagnosis Algorithm for Multiple Open-Circuited Faults of Microgrid Inverters Based on Main Fault Component Analysis," in *IEEE Transactions on Energy Conversion*, vol. 33, no. 3, pp. 925-937, Sept. 2018.

[9] P. G. Potamianos, E. D. Mitronikas and A. N. Safacas, "Open-Circuit Fault Diagnosis for Matrix Converter Drives and Remedial Operation Using Carrier-Based Modulation Methods," in *IEEE Transactions on Industrial Electronics*, vol. 61, no. 1, pp. 531-545, Jan. 2014.

[10] C. Gan, J. Wu, S. Yang, Y. Hu, W. Cao and J. Si, "Fault diagnosis scheme for open-circuit faults in switched reluctance motor drives using fast Fourier transform algorithm with bus current detection," in *IET Power Electronics*, vol. 9, no. 1, pp. 20-30, 20 1 2016.

[11] F. Zidani, D. Diallo, M. E. H. Benbouzid and R. Nait-Said, "A Fuzzy-Based Approach for the Diagnosis of Fault Modes in a Voltage-Fed PWM Inverter Induction Motor Drive," in *IEEE Transactions on Industrial Electronics*, vol. 55, no. 2, pp. 586-593, Feb. 2008.

[12] W. Sleszynski, J. Nieznanski and A. Cichowski, "Open-Transistor Fault Diagnostics in Voltage-Source Inverters by Analyzing the Load Currents," in *IEEE Transactions on Industrial Electronics*, vol. 56, no. 11, pp. 4681-4688, Nov. 2009.

[13] S. Khojet El Khil, I. Jlassi, A. J. Marques Cardoso, J. O. Estima and N. Mrabet-Bellaaj, "Diagnosis of Open-Switch and Current Sensor Faults in PMSM Drives Through Stator Current Analysis," in *IEEE Transactions on Industry Applications*, vol. 55, no. 6, pp. 5925-5937, Nov.-Dec. 2019.

[14] D. U. Campos-Delgado, J. A. Pecina-Sánchez, D. R. Espinoza-Trejo and E. R. Román Arce-Santana, "Diagnosis of open-switch faults in variable speed drives by stator current analysis and pattern recognition," in *IET Electric Power Applications*, vol. 7, no. 6, pp. 509-522, July 2013.

[15] H. Yan, Y. Xu, F. Cai, H. Zhang, W. Zhao and C. Gerada, "PWM-VSI Fault Diagnosis for a PMSM Drive Based on the Fuzzy Logic Approach," in *IEEE Transactions on Power Electronics*, vol. 34, no. 1, pp. 759-768, Jan. 2019.

[16] M. Trabelsi, M. Boussak and M. Benbouzid, "Multiple Criteria for High Performance Real-time Diagnostic of Single and Multiple Open-switch Faults in AC-motor Drives: Application to IGBT-based Voltage Source Inverter," Electric Power Systems Research, vol 144, 2017, Pages 136-149.

[17] Y. Cheng, Y. Sun, X. Li, H. Dan, J. Lin and M. Su, "Active Common-Mode Voltage-Based Open-Switch Fault Diagnosis of Inverters in IM-Drive Systems," in *IEEE Transactions on Industrial Electronics*, vol. 68, no. 1, pp. 103-115, Jan. 2021.

[18] T. Peng, H. Dan, J. yang and H. deng, "Open-Switch Fault Diagnosis and Fault Tolerant for Matrix Converter With Finite Control Set-Model Predictive Control," in *IEEE Transactions on Industrial Electronics*, vol. 63, no. 9, pp. 5953-5963, Sept. 2016.

[19] S. Khwan-on, L. de Lillo, L. Empringham and P. Wheeler, "Fault-Tolerant Matrix Converter Motor Drives With Fault Detection of Open Switch Faults," in *IEEE Transactions on Industrial Electronics*, vol. 59, no. 1, pp. 257-268, Jan. 2012.

[20] C. Brunson, L. Empringham, L. De Lillo, P. Wheeler and J. Clare, "Open-Circuit Fault Detection and Diagnosis in Matrix Converters," in *IEEE Transactions on Power Electronics*, vol. 30, no. 5, pp. 2840-2847, May 2015.

[21] H. Dan et al., "Error-Voltage-Based Open-Switch Fault Diagnosis Strategy for Matrix Converters with Model Predictive Control Method," in *IEEE Transactions on Industry Applications*, vol. 53, no. 5, pp. 4603-4612, Sept.-Oct. 2017.

[22] G. Zhang, H. Zhou, G. Wang, C. Li and D. Xu, "Current Sensor Fault-Tolerant Control for Encoderless IPMSM Drives Based on Current Space Vector Error Reconstruction," in *IEEE Journal of Emerging and Selected Topics in Power Electronics*, vol. 8, no. 4, pp. 3658-3668, Dec. 2020.

[23] G. Zhang, G. Wang, G. Wang, J. Huo, L. Zhu and D. Xu, "Fault Diagnosis Method of Current Sensor for Permanent Magnet Synchronous Motor Drives," 2018 *International Power Electronics Conference* (IPEC-Niigata 2018 -ECCE Asia), Niigata, 2018, pp. 1206-1211.

[24] G. F. H. Beng, X. Zhang and D. M. Vilathgamuwa, "Sensor Fault-Resilient Control of Interior Permanent-Magnet Synchronous Motor Drives," in *IEEE/ASME Transactions on Mechatronics*, vol. 20, no. 2, pp. 855-864, April 2015.

[25] G. Zhang, G. Wang, H. Zhou, C. Li, G. Wang and D. Xu, "Current Sensor Fault Diagnosis and Fault-Tolerant Control for Encoderless PMSM Drives Based on Dual Sliding-Mode Observers," 2019 *IEEE Applied Power Electronics Conference and Exposition*, Anaheim, CA, USA, 2019, pp. 2549-2553.

[26] M. Manohar and S. Das, "Current Sensor Fault-Tolerant Control for Direct Torque Control of Induction Motor Drive Using Flux-Linkage Observer," in *IEEE Transactions on Industrial Informatics*, vol. 13, no. 6, pp. 2824-2833, Dec. 2017.

[27] Y. Yu, Y. Zhao, B. Wang, X. Huang and D. Xu, "Current Sensor Fault Diagnosis and Tolerant Control for VSI-Based Induction Motor Drives," in *IEEE Transactions on Power Electronics*, vol. 33, no. 5, pp. 4238-4248, May 2018.

[28] X. Zhang, G. Foo, M. D. Vilathgamuwa, K. J. Tseng, B. S. Bhangu and C. Gajanayake, "Sensor fault detection, isolation and system reconfiguration based on extended Kalman filter for induction motor drives," in *IET Electric Power Applications*, vol. 7, no. 7, pp. 607-617, Aug. 2013.

[29] G. H. B. Foo, X. Zhang and D. M. Vilathgamuwa, "A Sensor Fault Detection and Isolation Method in Interior Permanent-Magnet Synchronous Motor Drives Based on an Extended Kalman Filter," in *IEEE Transactions on Industrial Electronics*, vol. 60, no. 8, pp. 3485-3495, Aug. 2013.

[30] T. A. Najafabadi, F. R. Salmasi and P. Jabehdar-Maralani, "Detection and Isolation of Speed-, DC-Link Voltage-, and Current-Sensor Faults Based on an Adaptive Observer in Induction-Motor Drives," in *IEEE Transactions on Industrial Electronics*, vol. 58, no. 5, pp. 1662-1672, May 2011.

[31] F. R. Salmasi and T. A. Najafabadi, "An Adaptive Observer With Online Rotor and Stator Resistance Estimation for Induction Motors With One Phase Current Sensor," in *IEEE Transactions on Energy Conversion*, vol. 26, no. 3, pp. 959-966, Sept. 2011.

[32] X. Wang, Z. Wang, Z. Xu, M. Cheng, W. Wang and Y. Hu, "Comprehensive Diagnosis and Tolerance Strategies for Electrical Faults and Sensor Faults in Dual Three-Phase PMSM Drives," in *IEEE Transactions on Power Electronics*, vol. 34, no. 7, pp. 6669-6684, July 2019.

[33] Z. Li et al., "A Fast Diagnosis Method for Both IGBT Faults and Current Sensor Faults in Grid-Tied Three-Phase Inverters with Two Current Sensors," in *IEEE Transactions on Power Electronics*, vol. 35, no. 5, pp. 5267-5278, May 2020.

[34] P. Cortes et al., "Guidelines for weighting factors design in Model Predictive Control of power converters and drives," 2009 *IEEE International Conference on Industrial Technology*, Churchill, VIC, Australia, 2009.

Hanbing Dan was born in Hubei, China, in 1991. He received the B.S. degree in Automation, and Ph.D. degree in Control Science and Engineering from Central South University, Changsha, China, in 2012, and 2017, respectively. He was a visiting researcher in Faculty of Engineering at the University of Nottingham, United Kingdom during 2017. He is currently an associate professor with the School of Automation, Central South University, China.

His research interests include power converter, motor control, model predictive control, fault diagnosis.

Wei Yue born in Hunan, China, in 1994. He received the B.S. degrees in electrical engineering and the automatization from School of Automation, Central South University, Changsha, China, in 2016.

He is currently pursuing the M.S. degree in electrical engineering at Central South University, Changsha, China. His research interests include model predictive control for permanent magnet synchronous motor and fault diagnosis.

Wenjing Xiong was born in Hunan, China, in 1991.She received the B.S. degree in Automation, and Ph.D degree in Control Science and Engineering from Central South University, Changsha, China, in 2012, and 2017, respectively. She is currently an associate professor with the School of Automation, Central South University, China.

Her research interests include modulation strategy for power converters, matrix converter, ac/dc converter and wireless power transfer.

Yonglu Liu (Member, IEEE) was born in Chongqing, China, in 1989. He received the B.S., M.S., and Ph.D. degrees in electrical engineering from Central South University, Changsha, China, in 2012, 2015, and 2017 respectively. He is currently an Associate Professor with School of Automation, Central South University, China.

His research interests include power electronics and renewable energy power conversion systems.

Mei Su (Member, IEEE) was born in Hunan, China, 1967. She received the B.S. degree in automation, the M.S. degree in automation, and the Ph.D. degree in control science and engineering from Central South University, Changsha, China, in 1989, 1992, and 2005, respectively. She has been a Full Professor with the School of Automation, Central South University. She is currently an Associate Editor of the IEEE Transactions on Power Electronics.

Her research interests include matrix converter, adjustable speed drives, and wind energy conversion system.

Yao Sun (Member, IEEE) was born in Hunan, China, in 1981. He received the B.S., M.S. and Ph.D. degrees from Central South University, Changsha, China, in 2004, 2007 and 2010, respectively. He has been a Professor with the School of Automation, Central South University, China.

His research interests include matrix converter, microgrid and wind energy conversion system.